Optoelectrofluidic Sandwich Immunoassays for Detection of Human Tumor Marker Using Surface-Enhanced Raman Scattering

ARTICLE *in* ANALYTICAL CHEMISTRY · SEPTEMBER 2010

Impact Factor: 5.64 · DOI: 10.1021/ac101325t · Source: PubMed

4 AUTHORS, INCLUDING:

Hyundoo Hwang
Tecnológico de Monterrey
44 PUBLICATIONS **659** CITATIONS
SEE PROFILE

Hyangah Chon
Hanyang University
17 PUBLICATIONS **640** CITATIONS
SEE PROFILE

Jaebum Choo
Hanyang University
207 PUBLICATIONS **4,907** CITATIONS
SEE PROFILE

Anal. Chem. **2010,** *82,* 7603–7610

Optoelectrofluidic Sandwich Immunoassays for Detection of Human Tumor Marker Using Surface-Enhanced Raman Scattering

Hyundoo Hwang,[†] Hyangah Chon,[‡] Jaebum Choo,*[,‡] and Je-Kyun Park*[,†,§]

Department of Bio and Brain Engineering, Korea Advanced Institute of Science and Technology (KAIST), 335 Gwahangno, Yuseong-gu, Daejeon 305-701, Republic of Korea, Department of Bionano Engineering, Hanyang University, 1271 Sa-1-dong, Sangnok-gu, Ansan, Kyeonggi-do 426-791, Republic of Korea, and KAIST Institute for the NanoCentury, 335 Gwahangno, Yuseong-gu, Daejeon 305-701, Republic of Korea

A sandwich immunoassay is a powerful tool for identifying a specific substance in a biological sample. However, its heterogeneous strategy always requires repetitive liquid handlings and long processing time. Here an optoelectrofluidic immunoassay platform for simple, fast, and automated detection of human tumor marker based on surface-enhanced Raman scattering (SERS) has been developed. By using a conventional optoelectrofluidic device and a liquid crystal display module, simple and quantitative detection of human tumor marker, alpha-fetoprotein, in a ~500 nL sample droplet has been automatically conducted with lower detection limit of about 0.1 ng/mL within 5 min. This study depicts the first practical application, for protein detection, of the optoelectrofluidic manipulation technology. This image-driven immunoassay platform opens a new way for simple, fast, automated, and highly sensitive detection of antigens.

Immunoassay, which is based on a specific interaction between an antigen and a complementary antibody, has become an important analytical tool for identifying and quantifying a specific substance in a liquid sample. In several fields such as clinical diagnosis, biochemical analysis, and environmental monitoring, many kinds of techniques, such as fluorescence, chemiluminescence, electrochemical methods, surface plasmon resonance, and enzyme-linked immunosorbent assay (ELISA), have been utilized to measure the antigens binding to its complementary antibodies. Recently, surface-enhanced Raman scattering (SERS) has also been applied to the immunoassays.[1−3] Among several kinds of SERS-based immunoassay methods, a sandwich immunoassay using metal nanoparticles labeled by a Raman-active probe has been most widely used because of its remarkable SERS-enhancement ability and good biocompatibility. Here, a sandwich immunocomplex is formed by immunoreaction between an antigen captured by antibodies immobilized on a solid substrate and probe-labeled metal nanoparticles. Then the antigen concentration can be indirectly determined by measuring the Raman intensity of the probe-labeled metal nanoparticles, which constitute the immunocomplexes in "sandwich" form.

For all the measurement techniques for the immunoassay including the SERS-based methods, this heterogeneous strategy always requires repetitive washing steps for separating antibody-bound and free proteins. In addition, a long incubation time is required for antibody−antigen binding reactions, which is limited by diffusion transport of molecules or nanoparticles. As a consequence, the manually conducted processes of a typical heterogeneous immunoassay, which involves multiple cycles of incubation and washing steps, usually take several hours and are labor-intensive. To deal these problems of a traditional immunoassay, many kinds of fully automated immunoassay analyzers, which can perform a various tests on a series of samples and process several batches simultaneously, have been commercialized. The automated systems usually take several tens of minutes for performing all steps, including sample dilution, dispensing, incubation, washing, and reading without manual handling of liquids except during the step for sample injection. However, the commercialized immunoassay instruments still have some limitations that they require massive and complicated constructions of robotic components and several hundreds of microliter sample volumes. Recently, microfluidic devices have also been applied for simple and rapid immunoassays in miniaturized system with small sample volumes.[4−6] Previous microfluidic immunoassay platforms, however, also require troublesome fluidic components, and yield large amount of dead volumes and many disposables.

Optoelectrofluidics, which is based on the electrokinetic motion of particles or fluids under an electric field induced by light, has attracted a great interest from many researchers in various fields of science and engineering. There are three well-known methods to optically induce electrokinetic motions in a fluid: (1) electrothermal vortex due to the thermal gradient induced by focusing

* To whom correspondence should be addressed. Fax: +82-42-350-4310. E-mail: jekyun@kaist.ac.kr(J.-K.P.); jbchoo@hanyang.ac.kr. (J.C.).

† Korea Advanced Institute of Science and Technology (KAIST).

‡ Hanyang University.

§ KAIST Institute for the NanoCentury.

(1) Porter, M. D.; Lipert, R. J.; Siperko, L. M.; Wang, G.; Narayanan, R. *Chem. Soc. Rev.* **2008**, *37*, 1001–1011.

(2) Han, X.; Zhao, B.; Ozaki, Y. *Anal. Bioanal. Chem.* **2009**, *6*, 285–297.

(3) Chon, H.; Lee, S.; Son, S. W.; Oh, C. H.; Choo, J. *Anal. Chem.* **2009**, *81*, 3029–3034.

(4) Jiang, X.; Ng, J. M. K.; Stroock, A. D.; Dertinger, S. K. W.; Whitesides, G. M. *J. Am. Chem. Soc.* **2003**, *125*, 5294–5295.

(5) Yager, P.; Edwards, T.; Fu, E.; Helton, K.; Nelson, K.; Tam, M. R.; Weigl, B. H. *Nature* **2006**, *442*, 412–418.

(6) Fan, R.; Vermesh, O.; Srivastava, A.; Yen, B. K. H.; Qin, L.; Ahmad, H.; Kwong, G. A.; Liu, C. C.; Gould, J.; Hood, L. *Nat. Biotechnol.* **2008**, *26*, 1373–1378.

10.1021/ac101325t
Published on Web 08/24/2010

a strong laser source;[7] (2) electrophoresis due to the local increment of current density by ultraviolet exposure of indium tin oxide (ITO);[8] and (3) optoelectronic tweezers (OET) based on a photoconductive layer deposited on a metal electrode.[9] The OET technology allows us to induce an electric field gradient in a fluid using a weak white light source, and to spatially modulate it using a conventional display device such as a liquid crystal display (LCD)[10] in a simple and easy way. By using the OET device, the image-based manipulation of several biological materials, which include blood cells,[10] oocytes,[11] swimming bacteria,[12] and biomolecules,[13,14] has been demonstrated. In addition, patterning of nonbiological objects such as polymer microspheres,[15] nanowires,[16] and metallic nanoparticles,[17] has been possible. Recently, a size-based separation of microspheres using the optoelectrofluidic platform has also been reported.[18]

Here a new immunoassay platform is developed for simple, rapid, and automated detection of proteins using a light-activated particle manipulation technology. By applying a conventional OET device to control antibody-conjugated polystyrene (PS) microspheres and probe-labeled silver nanoparticles (AgNPs), a SERS-based sandwich immunoassay of human tumor marker, alpha-fetoprotein (AFP), could be automatically performed using a programmed image from a conventional LCD module. This optoelectrofluidic immunoassay does not require any fluidic components and manual handling of liquids for all steps except for sample injection. Moreover, it requires only submicroliter sample droplet as a total specimen, and takes only several minutes to complete one assay cycle.

Theory. The electrokinetic mechanisms, which include dielectrophoresis (DEP) and ac electroosmosis (ACEO), are a main driving force for particle manipulation using an optoelectrofluidic device. In addition, we could also observe the electrostatic interactions due to the polarization of dielectric particles. DEP, one of the most widely applied principles for the optoelectrofluidic manipulation,[9−12,16,18,19] is the movement of dielectric objects under a nonuniform electric field driven by forces arising from the interaction between an induced electric dipole of the particle and the applied electric field.[20] The DEP force acting on a spherical particle is given by

$$F_{\mathrm{DEP}} = 2\pi r^3 \varepsilon_{\mathrm{m}} \mathrm{Re}[f_{\mathrm{CM}}] \nabla |E|^2 \quad (1)$$

where r is the radius of the particles; ε_{m} is the permittivity of the suspending medium; $\mathrm{Re}[f_{\mathrm{CM}}]$ is the real part of the Clausius−Mossotti factor. The value of $\mathrm{Re}[f_{\mathrm{CM}}]$ depends on the frequency of applied ac voltage and the conductivity of particles and medium, varying between +1 and −0.5. In the optoelectrofluidic device, the particles are repelled from the light pattern, where the electric field is relatively higher than other region, if $\mathrm{Re}[f_{\mathrm{CM}}]$ is negative (negative DEP). If $\mathrm{Re}[f_{\mathrm{CM}}]$ is positive, the particles move toward the light pattern (positive DEP).

The optically induced ACEO, which is a fluidic motion generated by the motion of ions within the electric double layer due to the tangential electric field, have also been applied for rapid concentration of microspheres, nanoparticles and molecules using an optoelectrofluidic device.[13,15,17,18] The fluids around the partially illuminated area in the optoelectrofluidic device flow along the surface of the photoconductive layer with a rectified slip velocity defined as shown:

$$\langle v_{\mathrm{slip}} \rangle_{\mathrm{t}} = \frac{1}{2} \frac{\lambda_D}{\eta} \mathrm{Re}[\sigma_{\mathrm{q}} E_{\mathrm{t}}^{*}] \quad (2)$$

where λ_D is the Debye length and η is the fluid viscosity. The charges contained in the Debye layer (σ_{q}) and the tangential electric field (E_{t}) vary sinusoidally and can be evaluated as $\sigma_{\mathrm{q}} = \varepsilon_{\mathrm{m}}\zeta/\lambda_{\mathrm{D}}$ and $E_{\mathrm{t}} = -\alpha\partial\zeta/\partial y$, respectively, where ζ is the zeta potential, which is the voltage drop across the Debye layer, and α is a geometry factor.[21]

In addition to these electrokinetic phenomena, electrostatic interactions among the microspheres due to their induced dipole are also observable. The electrostatic interaction force, $F_{\mathrm{dipole}} \propto r^6 \varepsilon_{\mathrm{m}} \mathrm{Re}[f_{\mathrm{CM}}]^2 E^2$, can make the particles form a structure like "perl chain" by attractive forces in the direction of an electric field, and a crystalline structure with a regular distances among the particles by repulsive forces in the plane perpendicular to the electric field.[22]

The electrokinetics mechanisms act on the microspheres in concert depending on the frequency of the applied ac signal.[18] For example, at the low-frequency range below 1 kHz, hydrodynamic drag force due to the strong ACEO flow becomes more dominant than other forces. The optically induced ACEO vortices make both micro- and nanosized particles move toward the illuminated area. While the nanoparticles tend to be always concentrated into the stagnation region, where the flows are converged, the microparticles sometimes move along the ACEO vortices on the edge of the light pattern in a certain condition depending on the applied ac signal, the light pattern, and the gravity force. At the high-frequency range above 10 kHz, the ACEO flow becomes much weaker; hence the DEP force becomes the most dominant force. Since most polymer microspheres show the negative DEP motion in low-conductivity media, they are repelled from the image patterns in the optoelectrofluidic device. Here the electrostatic dipole forces can also affect the behaviors of microparticles. On the other hand, the DEP force acting on the nanosized particles is negligible because the magnitude of

(7) Mizuno, A.; Nishioka, M.; Ohno, Y.; Dascalescu, L. D. *IEEE Trans. Ind. Appl.* **1995**, *31*, 464–468.
(8) Hayward, R. C.; Saville, D. A.; Aksay, I. A. *Nature* **2000**, *404*, 56–59.
(9) Chiou, P. Y.; Ohta, A. T.; Wu, M. C. *Nature* **2005**, *436*, 370–372.
(10) Hwang, H.; Choi, Y. J.; Choi, W.; Kim, S. H.; Jang, J.; Park, J.-K. *Electrophoresis* **2008**, *29*, 1203–1212.
(11) Hwang, H.; Lee, D.-H.; Choi, W.; Park, J.-K. *Biomicrofluidics* **2009**, *3*, 014103.
(12) Choi, W.; Nam, S.-W.; Hwang, H.; Park, S.; Park, J.-K. *Appl. Phys. Lett.* **2008**, *93*, 143901.
(13) Hwang, H.; Park, J.-K. *Anal. Chem.* **2009**, *81*, 5865–5870.
(14) Hwang, H.; Park, J.-K. *Anal. Chem.* **2009**, *81*, 9163–9167.
(15) Hwang, H.; Park, Y.-H.; Park, J.-K. *Langmuir* **2009**, *25*, 6010–6014.
(16) Jamshidi, A.; Pauzauskie, P. J.; Schuck, P. J.; Ohta, A. T.; Chiou, P. Y.; Chou, J.; Yang, P.; Wu, M. C. *Nat. Photonics* **2008**, *2*, 86–89.
(17) Jamshidi, A.; Neale, S. L.; Yu, K.; Pauzauskie, P. J.; Schuck, P. J.; Valley, J. K.; Hsu, H.-Y.; Ohta, A. T.; Wu, M. C. *Nano Lett.* **2009**, *9*, 2921–2925.
(18) Hwang, H.; Park, J.-K. *Lab Chip* **2009**, *9*, 199–206.
(19) Hwang, H.; Oh, Y.; Kim, J.-J.; Choi, W.; Park, J.-K.; Kim, S.-H.; Jang, J. *Appl. Phys. Lett.* **2008**, *92*, 024108.
(20) Jones, T. B. *Electromechanics of Particles*; Combridge University Press: New York, 1995.
(21) Probstein, R. F. *Physicochemical Hydrodynamics: An Introduction*; Wiley and Sons: New York, 1994.
(22) Hwang, H.; Kim, J.-J.; Park, J.-K. *J. Phys. Chem. B* **2008**, *112*, 9903–9908.

the DEP force is proportional to the volume of particles. Therefore, the nanoparticles move along the weak ACEO flows under the conditions. As the frequency decreases, the ACEO effect becomes stronger. The positive DEP force can sometimes attract the metallic nanoparticles, which were collected by ACEO flows and positioned near the surface, for immobilizing them onto the illuminated area.[17] In this high-frequency range, vortices due to the electrothermal effect are also observable with a strong light source. However, in our experimental condition, we could not observe the particle behaviors due to the electrothermal vortices.

EXPERIMENTAL SECTION

Sample Preparation for Fluorescence Immunoassay. Normal rabbit immunoglobulin G (rIgG)-biotin was obtained from Santa Cruz Biotechnology, Inc. (Santa Cruz, CA). Carboxylated fluorescent (Max. Ex/Em: 441/486) PS microspheres with diameter of 6 μm and neutravidin-coated fluorescent (Max. Ex/Em: 580/605) PS nanoparticles with diameter of 40 nm were purchased from PolySciences, Inc. (Warrington, PA) and Molecular Probes, Inc. (Eugene, OR), respectively.

After twice washing of PS microspheres with distilled ionized (DI) water, for the activation of other −COOH terminal groups on the PS microspheres, 10 μL of 10 mM *N*-hydroxysuccinimide (NHS) and 10 μL of 10 mM 1-ethyl-3-(3-dimethylaminopropyl) carbodiimide hydrochloride (EDC) were added to 470 μL of 10^8 particles/mL PS microspheres and allowed to react for 20 min. Then, 10 μL of 1.0 mg/mL monoclonal rIgG antibody (excess amount) was added to NHS-activated PS beads and reacted overnight at 4 °C. Here, unreacted antibodies were washed out by twice centrifuging, and the final PS microspheres with monoclonal rIgG antibody were redispersed in DI water.

Sample Preparation for SERS Immunoassay. For targeting AFP antigens, PS microspheres and SERS-active AgNPs were functionalized with monoclonal and polyclonal AFP antibodies, respectively. Here, 10 μL of 1.0 mg/mL monoclonal AFP antibody (excess amount) was added to NHS-activated PS beads and reacted overnight at 4 °C. Lastly, unreacted antibodies were washed out by twice centrifuging, and the final PS microspheres with monoclonal AFP antibody were redispersed in DI water.

Silver colloids were prepared by the method reported by Leopold and Lendl.[23] Here, silver nitrate was reduced by hydroxylamine hydrochloride. The detailed procedure for the preparation of AgNPs has been reported elsewhere.[24] Briefly, 5 mL of 3.0×10^{-2} M hydroxylamine hydrochloride was dissolved in 84 mL of triply distilled water and then 1 mL of 3.0×10^{-1} M sodium hydroxide was added to maintain an alkaline pH. Next, 10 mL of 2.0×10^{-2} M silver nitrate solution was added dropwise to the solution with continuous stirring. The solution was continuously stirred for an additional one day. UV/vis spectroscopy and transmission electron microscopy (TEM) were used to characterize the particle size of the produced colloids. The average particle size was determined to be 40 ± 10 nm.

To use these AgNPs as SERS-active probes, malachite green isothiocyanate (MGITC) was adsorbed onto the surface of the AgNPs. An amount of 1 μL of 5×10^{-5} M MGITC was added to 1 mL of AgNPs, and the mixture was reacted for 1 h under stirring. Then, dihydrolipoic acid (DHLA) was used for the antibody conjugation. The two -SH terminal groups of DHLA were chemically bonded to the silver surface. An amount of 2 μL of 5.0 mM DHLA was added to 1 mL of dye-adsorbed AgNPs and allowed to react for 1 h. Excess nonspecific binding mercaptoethanol in solution was removed by centrifuging the solution, and the precipitate was washed twice with DI water and resuspended.

For the activation of other −COOH terminal groups, 1 μL of 1.0 mM EDC and 1 μL of 1.0 mM NHS were added and allowed to react for 20 min. Finally, 1 μL of 1.0 mg/mL polyclonal AFP antibody (excess amount) was added to NHS-activated silvernanoparticles and reacted overnight at 4 °C. Unreacted NHS groups on the surface of the AgNPs were deactivated with 1 μL of 1.0 mM ethanolamine for 2 h. Nonspecific binding chemicals and antibodies were removed by centrifuging, and the final nanoprobes were washed twice with DI water.[3]

Device Configuration. A sample droplet, whose total volume is 500 nL (volume ratio of AFP antigens: PS microspheres: AgNPs = 1: 1: 1), was placed in a 30 μm-height liquid chamber of the optoelectrofluidic device, which consists of a bare ITO electrode and a photoconductive electrode. The height of the liquid chamber was fixed by photoresist gap spacers, which were fabricated on the bare ITO electrode using conventional photolithography. The photoconductive electrode was fabricated by sequential deposition of three layers: (1) a 50 nm-thick heavily doped hydrogenated amorphous silicon (a-Si:H); (2) an 1 μm-thick intrinsic a-Si:H, and (3) a 20 nm-thick silicon nitride on an ITO-coated glass substrate (Samsung-Corning Precision Glass, Korea) using a plasma enhanced chemical vapor deposition. The device surfaces were treated with 0.1% bovine serum albumin solution for about 30 min to reduce nonspecific adsorption of microspheres onto the device surface. Lastly, an ac voltage of 10 V_{pp} produced from a function generator (AFG310; Tektronix, OR) was applied across the ITO electrodes.

Experimental Setup for Optoelectrofluidic Immunoassays. Experimental setup for the optoelectrofluidic immunoassays is shown in Figure 1. A conventional inverted fluorescence microscope (IX71; Olympus Corp., Japan) was applied to construct the optoelectrofluidic immunoassay system. A monochromatic LCD module in a conventional projector (CP-S225; Hitachi, Japan) was mounted under the illumination lamp to generate a programmed image pattern for controlling an electric field. The LCD image was projected onto the photoconductive layer of the device through a condenser lens integrated into the microscope. The optoelectrofluidic device containing a sample droplet was put on the microscope stage as the transparent ITO electrode faces to the objective lens, since the photoconductive layer absorbs or blocks an incident laser beam and Raman scattering.

SERS Detection. SERS measurements were performed using homemade Raman microscope system. An inverted microscope IX71 (Olympus Corp.) was modified for sensitive Raman scattering detection. An Ar−Kr laser (Innova70C Spectrum, Coherent Inc., CA) operating at $\lambda = 647.4$ nm was used as the excitation source with a laser power of 5 mW. Raman scattering was collected using a charge-coupled device (CCD) camera at a spectral resolution of 2 cm^{-1}. Spectral measurements were made with a mono-

(23) Leopold, N.; Lendl, B. *J. Phys. Chem. B* **2003**, *107*, 5723–5727.
(24) Park, T.; Lee, S.; Seong, G. H.; Choo, J.; Lee, E. K.; Kim, Y. S.; Ji, W. H.; Hwang, S. Y.; Gweon, D. G.; Lee, S. *Lab Chip* **2005**, *5*, 437–442.

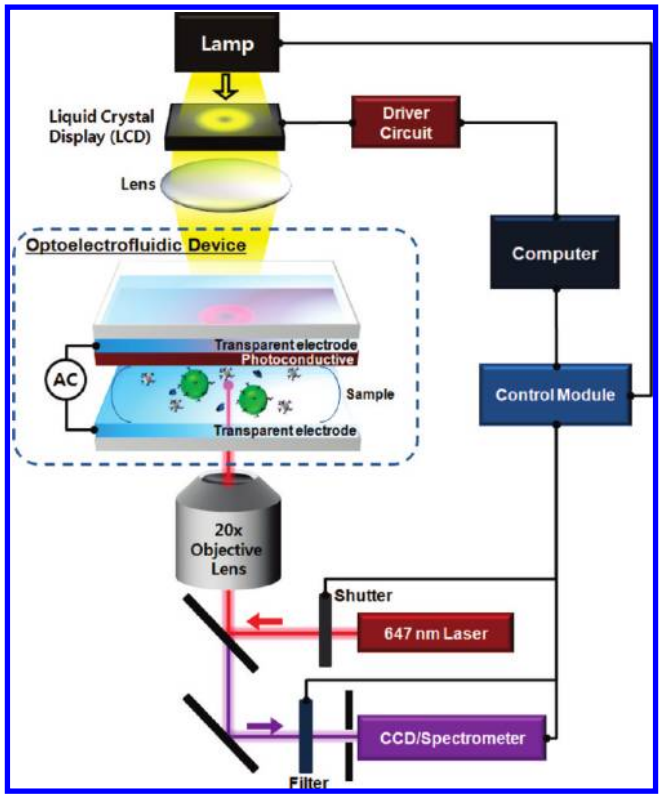

Figure 1. An experimental setup for optoelectrofluidic sandwich immunoassay. A conventional inverted fluorescence microscope was applied to construct the optoelectrofluidic immunoassay system. An LCD module was mounted under the illumination lamp to generate a programmed image pattern for controlling an electric field in a conventional optoelectrofluidic device.

chromator (Spectra 2500i, Princeton Instruments, Trenton, NJ). An additional CCD camera was fitted to an optical microscope to obtain optical images. Sandwich immunocomplexes in an optoelectrofluidic device were collected using a 20× objective lens was used to focus a laser spot on the glass. All of the Raman spectra reported here were collected for 2 s (integration time) in the range of 1050−1700 cm^{-1}.

Data Analysis. The fluorescence images were analyzed using ImageJ software (National Institute of Health, Bethesda, MD). The fluorescence intensity profiles were plotted with Origin (OriginLab, Northampton, MA). The SERS spectra were calibrated and analyzed using GRAMS (Thermo Fisher Scientific Inc., Waltham, MA). The calibration curve from the optoelectrofluidic immunoassay of AFP was fitted and plotted with Origin software.

RESULTS AND DISCUSSION

The image-driven immunoassay system based on the optoelectrofluidics is depicted in Scheme 1. After the sample injection step, there are four steps, which are automatically controlled by an applied ac signal and a programmed LCD image: (1) global concentration of supporting microspheres and mixing of the samples; (2) washing of free analytes and probe nanoparticles; (3) local concentration of the immunocomplexes; and (4) the optical measurement of the amount of probes on the immunocomplexes. At first, the suspended microspheres are concentrated due to DEP and ACEO induced by a programmed LCD image in the application of the ac signal, of which frequency is ranged from 1 to 100 kHz. At this step, as a dark circle becomes smaller gradually for a certain time, the efficient mixing of sample solution as well as the concentration of microspheres also arise by the ACEO vortices. This optoelectrofluidic mixing effect facilitates rapid formation of immunocomplexes. Here the time and efficiency for immunoreactions is controllable by programming the LCD image. After the animated image is fully processed and stopped in a form of a small dark circle, the ac frequency is changed into the range from 0.1 to 1 kHz for a few seconds. In the washing step, free probe nanoparticles are washed out from the dark area by the strong ACEO vortices and immobilized onto the photoconductive surface by the immobilization force, whereas the microspheres are concentrated into or still mixed with the other samples as moving along the ACEO vortices around the area due to the combination of ACEO, DEP and the gravity forces. When the applied ac frequency is changed into above 10 kHz, all the concentrated and washed immunocomplexes are concentrated and assembled into the dark area by the negative DEP forces and the electrostatic dipole interactions. Finally, an optical signal from the probe nanoparticles captured on the microspheres can be detected, after the applied voltage and the LCD image are turned off.

The process of image-driven automated immunoassay is shown in Figure 2. A programmed LCD image, in which a dark circle becomes smaller for about 90 s, was utilized for our experiments. The behavior of PS microspheres showed good agreement with the estimation based on the numerical simulation shown in Supporting Information Figure S1. The microspheres were successfully concentrated by the animated LCD image in the application of 1 kHz frequency. After the LCD image was stopped in a form of 50 μm-diameter dark circle, some concentrated microspheres were still moved along the ACEO vortices and mixed with other samples. When we changed the ac frequency from 1 kHz to 10 kHz, all the concentrated microspheres assembled and formed chain-like structure by the electrostatic interactions. Finally, we could detect SERS from the immunocomplexes by projecting a laser spot after turning off the LCD image and the ac voltage. The time for processing all the steps took less than 5 min. Here, the washing of free antigens and probe nanoparticles is also simultaneously processed, but it could not be determined this general optical observation. So, we determined the washing effect due to the optoelectrofluidics with fluorescence nanoparticles.

To investigate the feasibility of the optoelectrofluidic sandwich immunoassay, a qualitative experiment was performed with 0.1 ng/mL rIgG-biotin as a target analyte. Here fluorescent 6 μm-diameter PS microspheres conjugated with monoclonal anti-rIgG and neutravidin-coated fluorescent 40 nm-diameter PS nanoparticles were used as supporting substrates and probe nanoparticles, respectively. After the image-driven automated processes for the immunoassay of rIgG-biotin, we observed the fluorescence images of the processing area (Figure 3a). According to the microscopic pictures, the 6 μm-diameter supporting microspheres were successfully concentrated by the animated LCD image. In addition, the decrement of red fluorescence intensity within the microspheres-concentrated area was observed. This result might be due to the optoelectrofluidic washing of free fluorescent nanoparticles in the localized area. We also measured the intensity profile across

Scheme 1. Schematic Illustration of Procedures for Optoelectrofluidic Sandwich Immunoassays[a]

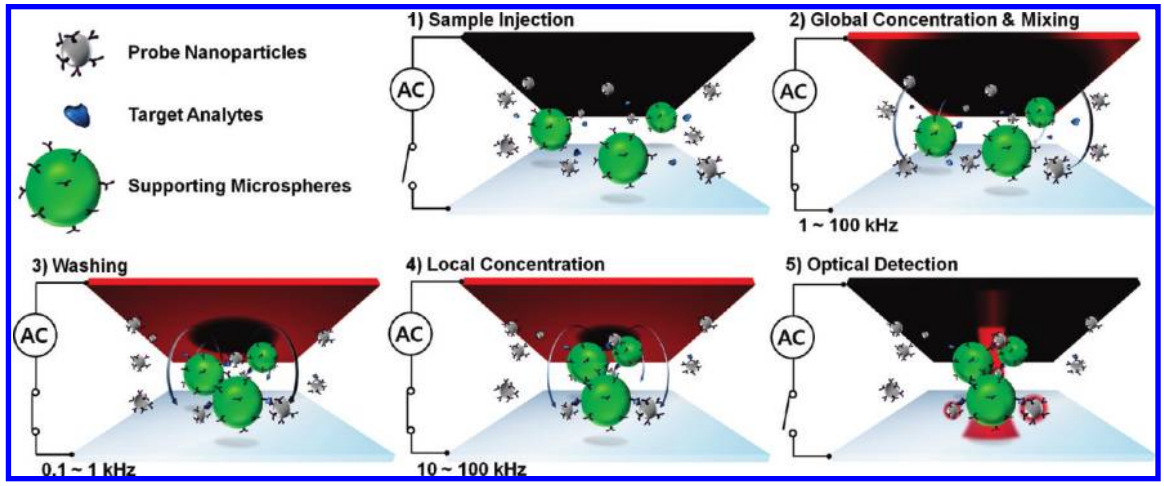

[a] The Raman probe-tagged metallic nanoparticles bind onto the supporting microspheres in the medium of target analytes, forming an immunocomplex. After all the processes, including sample concentration, mixing, reaction, and washing, are automatically conducted by a programmed LCD image, measurement of the amount of probe nanoparticles on the immunocomplexes is conducted with surface-enhaned Raman scattering (SERS).

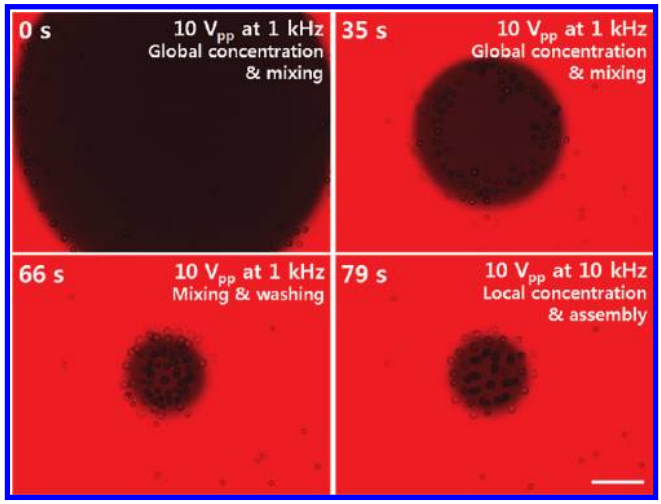

Figure 2. Microscopic pictures of PS microspheres being processed for optoelectrofluidic immunoassay. At 1 kHz, an animated LCD image concentrates the microspheres by ACEO vortices and negative DEP forces. After the animation stops, the strong ACEO flows mix the concentrated microspheres with target analytes and probe nanoparticles, and wash free molecules and nanoparticles from the dark area. At 10 kHz, the washed immunocomplexes are assembled and concentrated into the area for detection of SERS. Scale bar = 25 μm.

the microspheres inside and outside the washed area. Within the washed area, red fluorescence was appeared only on the same position of concentrated microspheres in the washed area as shown in Figure 3b. The intensity of fluorescence signal implies the amount of fluorescent nanoparticles, which formed sandwich immunocomplexes through the medium of rIgG-biotin molecules. While on the other, in the case of a microsphere, which was failed to concentrate and wash, the measurement of red fluorescence from the probe nanoparticles, which bound on a supporting microsphere, was impossible due to the interference by large amount of free probe nanoparticles around the microspheres as shown in Figure 3c. These results ensure that the mixing, concentration, and washing steps for immunoassay can be conducted by the image-driven automated processes.

It was also possible to form a microarray composed of numerous virtual wells using a programmable LCD image as shown in Figure 4a. This result shows that the multiplexed immunoassays could be conducted on the basis of individual microspheres in each well. Multiple SERS immunoassays could also be simultaneously performed by applying an LCD image, which generates multiple number of virtual wells (dark circles) for concentration and washing immunocomplexes (Figure 4b). If the amount of probe nanoparticles is quantified using a microscopic picture for the multiplexed immunoassays, the amount of immunocomplexes concentrated into the virtual wells should be consistent for accurate quantitative analysis or the optical signal from the probe nanoparticles should be normalized with that from the supporting microspheres. In our experimental condition, however, where the SERS-based detection was performed using a laser spot, there is no trouble in quantification if the number of the concentrated microspheres exceeds the minimum amount for filling the focal volume of the incident laser.

The quantitative assay of human AFP based on SERS was performed using this optoelectrofluidic immunoassay platform. Here, monoclonal anti-AFP-conjugated 6 μm-diameter PS microspheres were used as supporting material, and polyclonal AFP antibody-conjugated 40 nm-diameter AgNPs, which are labeled with malachite green isothiocyanate (MGITC) molecules as Raman probe, were utilized as SERS-probe nanoparticles (Figure 5a). The SERS spectra of the sandwich immunocomplex against various concentrations of AFP are illustrated in Figure 5b. Since the SERS intensities of AFP and antibodies were negligible compared to those of MGITC (see Supporting Information Figure S2), the amount of AFP antigens could be quantified by measuring the SERS signal of MGITC. The concentration of AFP was varied from 0.1 to 1.5 ng/mL. The SERS signals were obviously increased as the concentration of AFP increased. The blank spectrum was obtained without the target antigen. The weak SERS signal in the absence of antigens implies that some MGITC-tagged AgNPs still remained in the washed area or were nonspecifically bound onto the microspheres. Among several prominent peaks in the spectrum of MGITC, the peak at 1615 cm^{-1} was chosen for the quantitative evaluation of AFP antigens, because the baseline

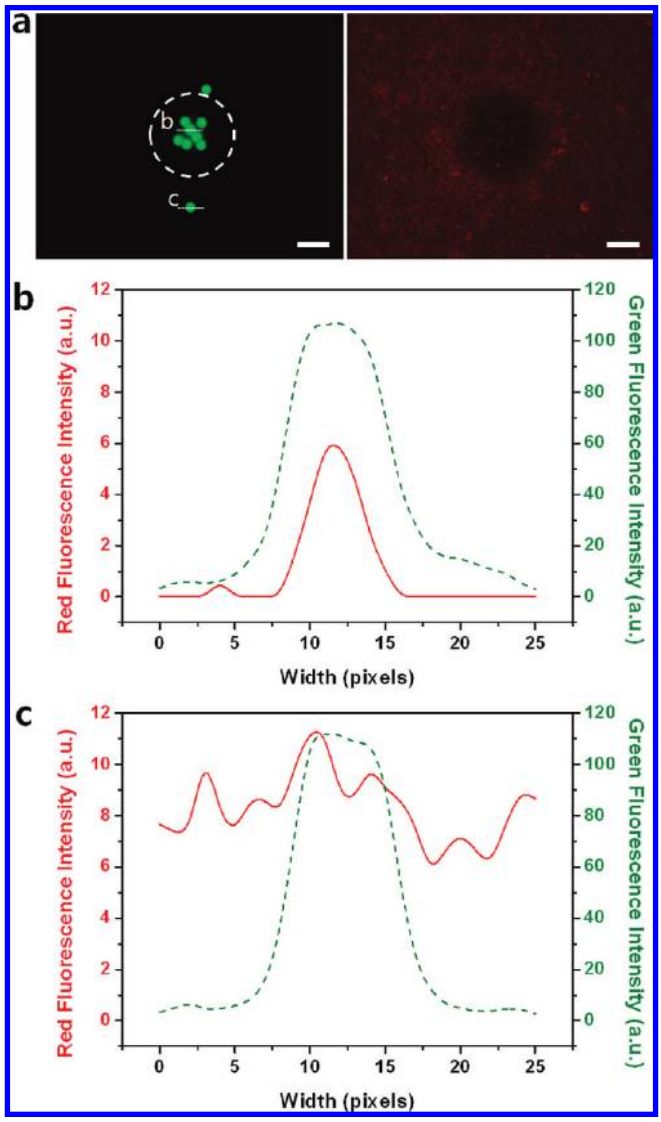

Figure 3. Optoelectrofluidic sandwich immunoassay for rIgG-biotin. (a) Microscopic pictures after all steps for optoelectrofluidic immunoassay against the emission wavelength (left: green, right: red). The dotted circle is a dark area of the LCD image, which the microspheres are concentrated into and the nanoparticles are washed out from. The fluorescence intensity profiles of a microsphere (b) inside and (c) outside the washed area across the dotted line in panel a. Red solid line and green dotted line depict the fluorescence intensity profiles of the immunocomplex according to the emission wavelengths of probe nanoparticles and supporting microspheres, respectively. Scale bar = 25 μm.

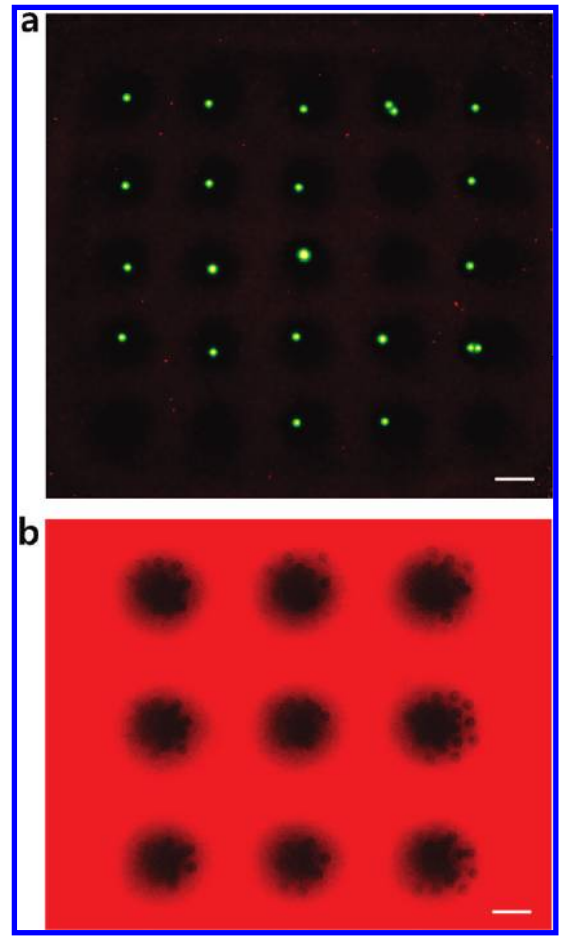

Figure 4. Simultaneous multiple experiments using a microarray pattern. (a) A 5 × 5 microarray composed of numerous virtual wells, in which fluorescent microspheres were trapped. Free probe nanoparticles (red) were successfully washed out from individual microspheres (green) which are trapped in each well. (b) Microspheres concentrated into and assembled within a 3 × 3 microarray after simultaneous multiple SERS-based immunoassays using a programmable LCD image. Scale bar = 25 μm.

of this peak (1555−1640 cm^{-1}) was flatter than others. The intensity of the peak was plotted as a function of the AFP concentration in Figure 5c. The Raman peak intensity linearly increased, as the concentration of AFP increased from 0 to 1.5 ng/mL. The equation for the linear regression line was $y = 3302x + 216.9$, and the correlation coefficient (R) was 0.9910 ($n = 6$). The lower detection limit (LDL) of this optoelectrofluidic SERS-based immunoassay for AFP was 98 pg/mL, which is twenty times lower than that of the conventional ELISA methods. This optoelectrofluidic immunoassay platform required total sample volume of less than 500 nL, which is much less than that for ELISA. In addition, the time for one assay took less than 5 min, and manual handling of liquids was not required except for injecting samples into the glass slide-like OET device. This time for automated immunoassays is one hundred times shorter than that for performing manual immunoassay of AFP using conventional ELISA.

According to the calibration curve shown in Figure 5c, not only the value of peak intensity, but also the standard deviation increased as the antigen concentration increased over 1 ng/mL. When the AFP concentration was over 2 ng/mL, the reproducibility of SERS signal was significantly decreased. These phenomena might be due to the aggregation of MGITC-tagged AgNPs by AFP solution. We could optically determine the silver aggregates, of which size is over several hundreds of nanometer, as soon as we injected the 2 ng/mL AFP solution. The large silver aggregates were also concentrated into the dark area and were not washed completely. However, this matter is not restricted to the case of this optoelectrofluidic immunoassay platform. In practice, most of the SERS-based biosensors have such the problems due to the aggregation of metal nanoparticles. If the limitation of SERS technology can be overcome, broader dynamic range of the immunoassay would be obtained.

Even in the absence of AFP, a weak SERS signal was observed in Figure 5b. There are two reasons: (1) some probe nanoparticles

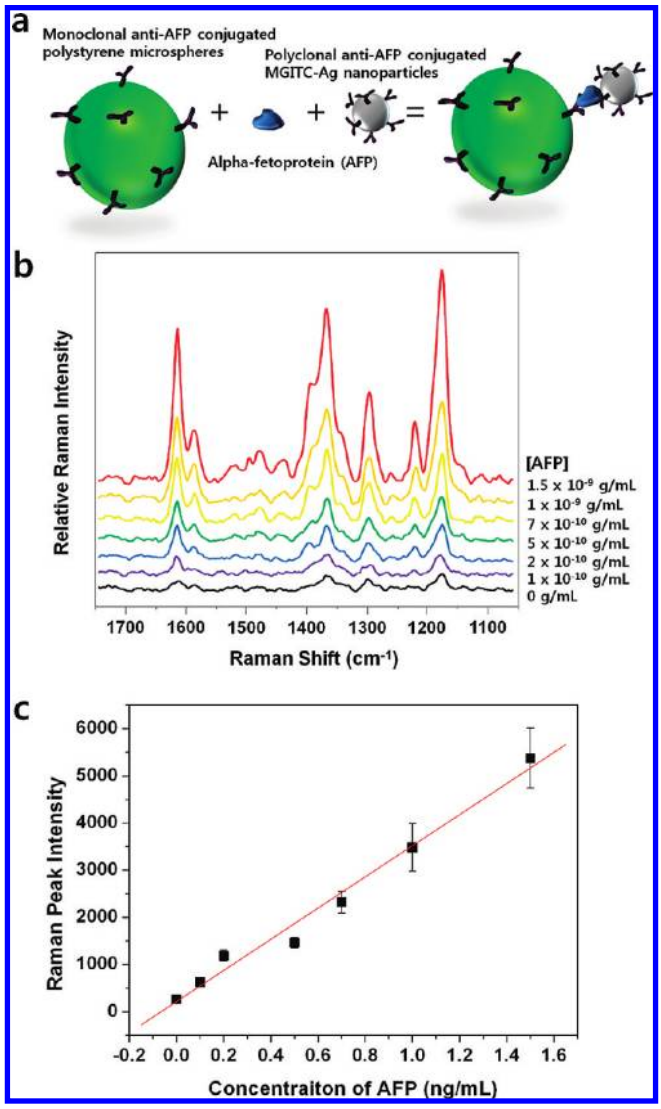

Figure 5. The quantitative assay of human AFP based on optoelectrofluidic SERS. (a) Schematic illustration of the formation of immunocomplex for SERS-based assay. Human AFP and MGITC-tagged AgNPs were applied for target analytes and probe nanoparticles, respectively. (b) SERS spectra for various concentrations of AFP antigen. (c) Intensity of the SERS signal at 1615 cm^{-1} against the concentration of AFP. A linear relationship is shown in the concentration range from 0 to 1.5 ng/mL. The linear fitting line is $y = 3302x + 216.9$, and $R = 0.9910$ ($n = 6$).

still remained in the washed area; (2) nonspecific binding of antigens or probe nanoparticles onto the microspheres. The former might be due to the behavior of nanoparticles by optoelectrofluidic flows and thermal motion. Most of the nanoparticles were washed out from the dark image and immobilized into the illuminated area. According to the simulation depicted in Supporting Information Figure S1, however, there was still weak flow converging into the dark area along the bare ITO surface. The flow is originated from the main ACEO flow toward the illuminated area along the photoconductive surface. Although the strong electrohydrodynamic flow washed out the free nanoparticles and molecules, little influx of probe nanoparticles might be slowly occurred. The thermal motion of the washed nanoparticles after turning off the voltage at the detection step can also affect the background signal. However, according to our experiments with fluorescent nanoparticles and the previous literature,[17] the dispersion of washed or patterned nanoparticles due to their Brownian motion was negligible. The latter, which is relative to the nonspecific absorption of antigens and nanoparticles, may be caused by electrostatic forces as well as by chemical binding forces. In-depth consideration for the electrostatic particle−particle interactions in this optoelectrofluidic immunoassay was discussed as follows.

At the ac frequencies ranged from 1 to 100 kHz, which include our experimental conditions, the electrostatic particle−particle interactions due to the induced-dipole of microspheres were observed. The attractive force, which aligns the microspheres in the direction of electric field, became stronger at 10 kHz than at 1 kHz, resulting in the "perl chains" of concentrated microspheres. This chain structure of immunocomplexes facilitated the highly sensitive detection of antigens by increasing the amount of probe nanoparticles exposed to the focal volume of the incident laser. If the microspheres are assembled in a monolayer, the SERS from only one immunocomplex will be detected. However, in this experimental condition, at least three to five 6 μm-diameter microspheres form a chain, of which length is enough to cover the focal volume ($\sim 10^{-17}$ m^3) of the incident laser, in the direction of the beam. In addition, the contact points among the microspheres in a chain can serve as hot spots for enhancing SERS signal from the probe nanoparticles. However, this chain structure may interfere with the reproducible SERS detection. The chain began to relax as soon as turning off the applied voltage for SERS detection. As a consequence, the SERS signal gradually reduced with a large fluctuation from about 30 s after the ac signal was intercepted. Therefore, we could obtain reproducible SERS intensity for only 30 s after the voltage is turned off.

The electrostatic interactions may also induce nonspecific binding of probe nanoparticles onto the microspheres. However, according to our experiments with fluorescence, the electrostatic attraction between microspheres and nanoparticles was observable only at extremely low-frequency range around 100 Hz (data not shown). Therefore, the electrostatic binding of nanoparticles onto microspheres would be negligible in our experimental conditions ranged from 1 to 10 kHz. However, it is difficult to conclude that there is no nonspecific binding of probe nanoparticles by electrostatic interactions yet, thus this matter should be investigated and solved for lower detection limit.

CONCLUSIONS

In this article, an optoelectrofluidic immunoassay platform has been developed for simple, automated, fast (~5 min), and highly sensitive (LDL = 98 pg/mL) detection of AFP in tiny sample volume (~500 nL) using SERS. This image-driven immunoassay using a conventional OET device has five significant meanings in several perspectives. First, this paper demonstrated the first application for detecting biological molecules using an optoelectrofluidic device. Up to now, all the studies about optoelectrofluidics have been focused only to the manipulation of some objects, except only one study about applying an OET device for the measurement of molecular diffusion coefficient.[14] In such a context, the optoelectrofluidic immunoassay has a significant meaning in respect that this is the first realization of the detection technology based on optoelectrofluidics. Second, much less

volume of samples was required for the assay than the conventional ELISA systems. Only a several hundreds of nanoliter sample droplet, which contains supporting microspheres, target analytes, and probe nanoparticles, was dropped on the OET device for the immunoassay in this system. Third, any complicated robotic or fluidic components were not required for the automated immunoassays. Only an OET device, which is similar to a glass slide, and an LCD module for controlling fluids were required. This simple structure and cheap components make it easy to commercialize and apply this technology for clinical diagnosis and biochemical analysis. Fourth, by using the optoelectrofluidic immunoassay, it took much less time (~5 min) to conduct all the processes for sandwich immunoassay than conventional methods. The incubation time shortened due to the enhanced mixing effect by the optically induced electrohydrodynamic vortices, as well as the fully automated processes without pipetting liquid samples allows us to save times. Finally, the image-driven manipulation platform allows more flexible uses of this technology. For example, parallel multiple assays were possible based on an LCD image programmed for generating multiple areas for concentration, reaction, washing, and detection. Based on this approach, a new multiplexed immunoassay platform could be constructed using an array of optically controlled virtual microwells.

Some challenges also remain. First, the performance of this optoelectrofluidic technology is basically dependent on the conductivity of media. For a salty media such as blood plasma or cell culture media, the photoconductivity should be much higher than the conventional OET device based on amorphous silicon. The phototransistor-based OET device could be utilized for increasing the photoconductivity of the device and applying this technique for high-conductivity physiological buffers.[25] Second, the performance depends on the applied ac frequency as well. A process for optimization of the ac frequency condition, therefore, is always required before applying different probe nanoparticles. For example, the silver nanoparticles were washed well and immobilized onto the illuminated area at higher frequency above 1 kHz, whereas relatively low ac frequency from 100 Hz to 1 kHz was optimized condition for the fluorescent polymer nanoparticles. Third, thick glass substrate and opaque photoconductive layer can interfere with the effective measurement of optical signals as well as flexible modification of optical pathway. This limitation could also be overcome by developing a new device or by applying sensitive probes for more flexible and sensitive optical detection. Finally, the integration of microfluidic components for manipulating multiple sample solutions would be very helpful for embodying immunoassays of multiple targets or conducting more complicated processes. Such the research for integrating microfluidic channels into the optoelectrofluidic device has already been performed.[26] Despite these challenges and limitations, the optoelectrofluidic sandwich immunoassays have fascinating meanings in the perspectives that it provides a new way for simple, fast, automated, and highly sensitive detection of antigens, and it is the first practical application for protein detection based on the optoelectrofluidic manipulation.

ACKNOWLEDGMENT

This research was supported by the National Research Laboratory (NRL) Program grant (R0A-2008-000-20109-0) and by the Nano/Bio Science and Technology Program grant (2008-00771) through the National Research Foundation of Korea funded by the Ministry of Education, Science and Technology (MEST). We also thank the TFT-LCD Research Center, Kyung Hee University, Korea. J.C. acknowledges the National Research Foundation of Korea (R11-2010-044-1002-0) for financial support. H.H. and H.C. contributed equally to this work.

SUPPORTING INFORMATION AVAILABLE

Simulation study (Figure S1) and SERS spectra (Figure S2). This material is available free of charge via the Internet at http://pubs.acs.org.

Received for review May 20, 2010. Accepted August 13, 2010.

AC101325T

(25) Hsu, H.-y.; Ohta, A. T.; Chiou, P.-Y.; Jamshidi, A.; Neale, S. L.; Wu, M. C. *Lab Chip* **2010**, *10*, 165–172.

(26) Lee, D.-H.; Hwang, H.; Park, J.-K. *Appl. Phys. Lett.* **2009**, *95*, 164102.